Repeatability and Accuracy of Laser Scanning-Based Reverse Engineering for Warped Composite Components

Eric J. Martin[1], O. Remus Tutunea-Fatan[2], Ryan Gergely[3] and David A. Okonski[4]

[1]Western University, emarti58@uwo.ca
[2]Western University, rtutunea@eng.uwo.ca
[3]General Motors, ryan.gergely@gm.com
[4]General Motors, david.a.okonski@gm.com

Corresponding author: O. Remus Tutunea-Fatan, rtutunea@eng.uwo.ca

Abstract. The dimensional accuracy of warped composite parts can be difficult to assess because they are characterized by relatively large deviations in different directions. The distorted shape of the part poses significant fixturing challenges. The present study discusses several scanning strategies with a focus on their resulting accuracy and repeatability. The overall results suggest that while the sources of error introduced in the reverse engineering process cannot be totally eliminated, the accuracy and repeatability of the process can be brought into acceptable ranges if parts are scanned by placing them in a free state on a quasi-flat surface.

Keywords: Laser Scanning, Reverse Engineering, Accuracy, Repeatability, Composite, Warpage, Dimensional Accuracy, Manufacturing, Compression Molding.
DOI: https://doi.org/10.14733/cadaps.2021.1018-1034

1 INTRODUCTION

Undoubtedly, coordinate measurement machines (CMM) have been the 'gold standard' in part inspection for several decades. Nonetheless, owed to the improvements in non-contact data acquisition, laser scanners have begun to replace CMMs in many applications including the restoration of cultural artifacts as well as in medical applications [7],[14]. One of the key advantages of laser scanners over CMMs is their ability to scan more complex geometries faster [8],[15] as well as their generic applicability to deformable parts. However, the accuracy of laser scanners remains relatively low compared to their physical contact counterparts [1],[4],[6],[10-13]. In many studies, CMM was used as the primary validation tool, a route enabled by the high rigidity of the validation sample, typically made of metal. Similarly, Besic et al [2] attempted to improve the accuracy of the line scanning process by using advanced filtering operations in order to obtain a better agreement between the non-contact and contact (CMM) results.

The growing number of composite automotive components that are being incorporated in practically every vehicle in order to meet more and more stringent emission standards has brought up new issues with respect to the assessment of part quality. Among them, the difficulties associated

with the fixturing of warped parts represent some of the most significant challenges to be overcome. The randomness and magnitude of the warpage pattern resulting from high-volume composite manufacturing processes makes the use of conventional fixtures with fixed datums very challenging. The geometric constraints imposed by the fixed location of the datums can alter the entire 'free-state' warpage pattern and hence yield irrelevant post-fixturing measurements. Along the same lines, the simple placement of the warped workpiece on an inspection table will render the CMM useless since the unstable part is prone to move under the action of the measuring probe.

This study is focused on compression molded composite parts that are characterized by relatively large warpage patterns (up to 7 mm deviation from the nominal shape) as well as a high degree of part-to-part variability. In this context, the main objective of this work was the identification of an accurate and repeatable non-contact measuring technique capable of determining the "free-state" warpage of these parts.

2 GENERAL FRAMEWORK

The main goal of this study was to assess the accuracy and repeatability of the laser scanning-based reverse engineering (RE) procedure as applied on glass-fiber reinforced parts produced through compression molding. Since the two test components shown in Figure 1 – identified as seatback outer (SBO) and seatback inner (SBI) - are to be assembled through ultrasonic welding, the gaps between their interior and exterior flanges have to be assessed prior to the assembly phase of the manufacturing process. Furthermore, a warpage-based output metric was used to determine an optimal set of molding conditions. In this context, the accuracy of the RE and dimensional assessment procedure is of paramount importance since it affects both upstream and downstream decisions along the manufacturing chain.

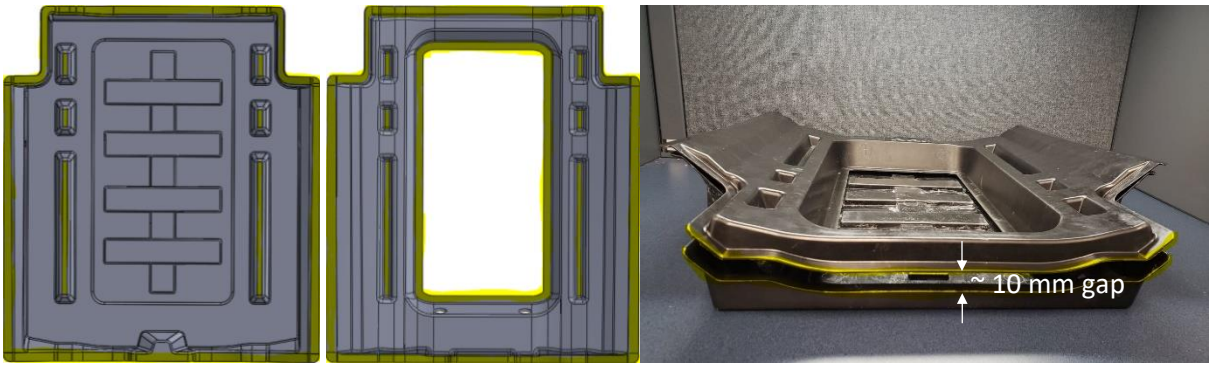

Figure 1: Sample parts with welding areas highlighted in yellow: (a) seatback outer (SBO), (b) seatback inner (SBI), (c) pre-assembly positioning of SBO (bottom) & SBI (top).

A Faro EDGE laser line probe (LLP) portable scanning arm (calibrated values: accuracy ±25 μm, repeatability 25 μm) was used to acquire part geometry point cloud data. To assess the errors accumulated in the RE process, a study on the repeatability and accuracy of the results was performed according to the assessment plan depicted in Figure 2. For reference purposes, the dimensions of the bounding box for both composite components were 540 x 480 x 98 mm with a thickness varying between 2.0 and 3.9 mm.

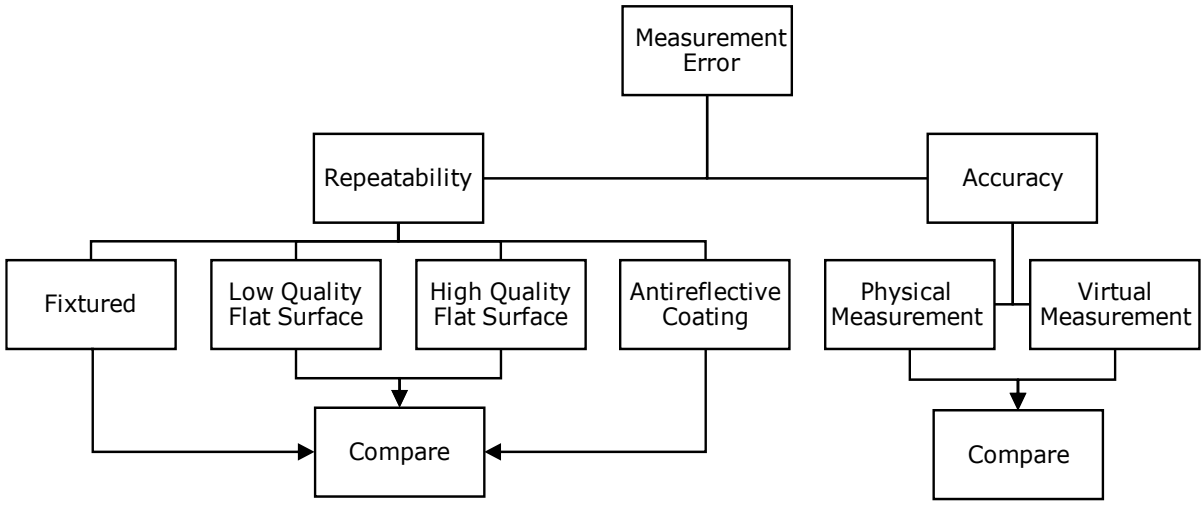

Figure 2: Error assessment plan.

3 CASE STUDY: COMPLEX GEOMETRY

3.1 Repeatability Assessment

The repeatability of each different RE procedure was evaluated under the same testing conditions and by involving the same data acquisition process. First, clouds of points were acquired by means of a laser scanner. For this purpose, a predetermined scan path was followed by the scanner operator in order to ensure the perpendicularity of the incident laser beam with the scanned surface. The optimal focal distance to the surface was monitored by the scanning equipment and visual cues were provided for operator guidance. Evidently, it is reasonable to expect that the inherent manual nature of the scanning operation introduces a certain degree of the variability in the acquired data, but its magnitude was relatively low. Following this, the overlapping scanning paths were automatically registered to each other and eventually merged into a single set of data. For the data collected in this study, the maximum allowable merging distance was set to 2 mm and the number of iterative blending steps was set to 15. These settings were meant to ensure smooth transitions between the overlapping scan passes in order to minimize the inherent deviations associated with adjacent scanning passes. These points were then filtered in the reverse engineering software by means of a user-set standard deviation (0.025 mm) that was determined heuristically. This value provides a threshold at which any points outside of the commonly used range ($\pm 3\sigma$) are being removed on the basis of being outliers. Evidently, if the value of σ is set too small, then many of the scanned points will be filtered out and the geometry will become difficult to repair due to the numerous defects (i.e., 'holes') introduced in the acquired data. Conversely, if the selected standard deviation is too large, too many outliers will be retained and thereby too much 'noise' will be introduced in the data. According to the trial-and-error tests performed on the analyzed geometries/parts, the chosen value (0.025 mm) – while subjective – appeared to strike a good balance between the completeness and smoothness of the post-filtering data.

After filtering, point cloud data was converted into a triangular mesh. Additional mesh generation controls were used to further improve the quality of the mesh. In this regard, a small rolling ball of 0.5 mm radius was used to further smoothen the geometry and a low reduction rate (2%) was applied in order to improve the flatness of the small near-planar areas that were visible in the data. Larger ball radii could alter the innate fillets/curved regions of the geometry whereas larger decimation rates could inadequately flatten non-planar areas. Same as in the prior step, both

parameters were determined through heuristic searches and therefore they are likely only applicable to the geometry analyzed in the present context.

After the completion of the data post-processing phases, two scans of the same part were aligned to each other by employing a conventional best-fit technique. According to the known principles, the best-fit alignment technique aims to minimize all distances between the two geometries to be compared. Owed to the previously mentioned post-processing parameters that were kept consistent for all reconstructed geometries, the best-fit alignment method yielded repeatable results. More specifically, the minor post-processing artifacts that were still present in the geometry did not affect the quality of the relative positioning/alignment between the pair of geometries to be compared. This could also be regarded as a consequence of the global - rather than local - nature of the comparison involved in the best-fitting approaches that essentially allowed elimination of the possible perturbations to be introduced by small data artifacts/defects. The robustness and stability of the best fitting technique was also warranted by the large density of scanned points that were originally acquired: approximately 2M points for SBO and 1M for SBI.

Once the alignment was completed, then differences (termed deviations) between these two scans were measured and exported as tabulated numerical values. Finally, the standard deviation and range of these values were calculated and used to assess the match between pairs of scans. The following sections present several different techniques used to investigate the repeatability.

3.1.1 Fixtured scanning

To evaluate the effect of fixturing on part warpage, the part was vertically mounted in a fixture whose primary functional was to allow a facile scanning of both A and B-sides of the part (Figure 3a). The fixture was designed with telescopic arms to accommodate the scanning of parts of various dimensions and at different laser scanner heights. The resulting standard deviation was ±0.56 mm. As suggested by Figure 3b, the consistency of the acquired scan data is relatively low with error in both positive and negative directions. The deviations ranged from a maximum of +1.514 mm and a minimum of -1.992 mm.

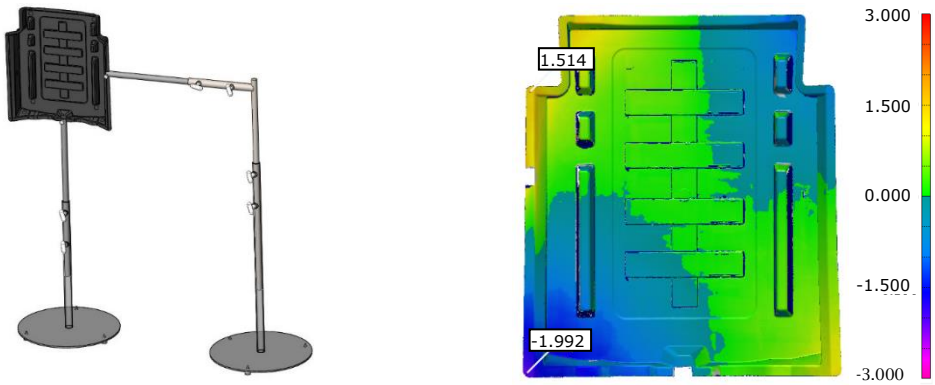

(a) (b)

Figure 3: Repeatability evaluation in the ”fixtured” scenario: (a) overview of the fixturing setup, (b) sample deviation map between two replicate scans (mm).

3.1.2 Free-state scanning on a low-quality flat surface

In an effort to improve RE repeatability, alternative scanning and part fixturing schemes were investigated. First, one side of the test part was scanned while at rest on the ‘flat’ surface of a common stainless-steel laboratory table. Since no fixturing was used, the part was in its free, but warped post-compression molding state. The resulting standard deviation was reduced to ±0.087 mm compared to the previous setup. The deviations ranged from a maximum of +0.216 mm

and a minimum of -0.279 mm (Figure 4a).

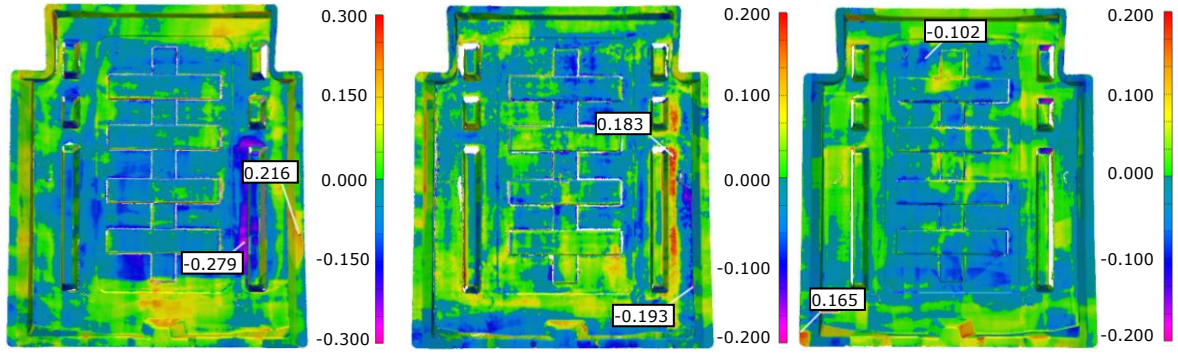

(a) (b) (c)

Figure 4: Sample paired comparisons between replicate scans (mm): (a) unclamped on low quality flat surface, (b) unclamped on high quality surface, (c) scenario (b) covered with antireflective coating.

3.1.3 Free-state scanning on a high-quality flat surface

Since both the stability and the flatness of the laboratory table were questionable, the prior laser scanning experiments were repeated on a high-quality laboratory table whose principal component was a granite slab. The resulting standard deviation was further reduced to ±0.059 mm. The deviations ranged from a maximum of +0.183 mm and a minimum of -0.193 mm (Figure 4b).

3.1.4 Antireflective coating

To evaluate the possibility of further enhancing the repeatability of the scanning operation, an opaque white powder was applied in order to reduce/eliminate the artifacts introduced by the black and reflective surface of the composite parts. Reflective parts can introduce outliers which would impact accuracy; additionally, the outlier formation is dependent on the angle of the scanner compared to the surface [16]. This random distribution of outlier points could also have a negative impact on repeatability. After a new set of scans were performed in the free-state on the granite table, the resulting standard deviation was again further reduced to ±0.047 mm. The deviations ranged from a maximum of +0.165 mm and a minimum of -0.102 mm (Figure 4c). While the antireflective coating was applied in a manual and thus error prone manner, it is unlikely to expect that the concievable nonuniformity of the applied layer would influence the quality of the acquired data in a significant manner. Furthermore, the thickness of the coating is too small to affect the dimensional accuracy of the data acquired. Nonetheless, future studies on this topic could validate these inherent assumptions.

3.1.5 Discussion

A summary of the discrepancies measured between pairs of replicate scans is presented in Table 1. Here, "StDev" is one standard deviation (σ) of the measured deviations between two replicate scans. This data suggests that repeatability is best ensured by coating parts with an antireflective coating and scanning in a free-state while resting on a high-quality granite table.

Fixtured	**Free-state**		
	Low Quality Flat Surface	**High Quality Flat Surface**	**Coated on High Quality Flat Surface**
StDev [mm]	**StDev [mm]**	**StDev [mm]**	**StDev [mm]**
0.560	0.087	0.059	0.047

Table 1: Summary of repeatability results for different scenarios.

Similarly, the overlays between replicate scans depicted in Figure 5 suggest that the percentage of points outside of the preset range of the deviation map (±0.1 mm) – presented in gray color - decreases as the repeatability of the scanning technique increases.

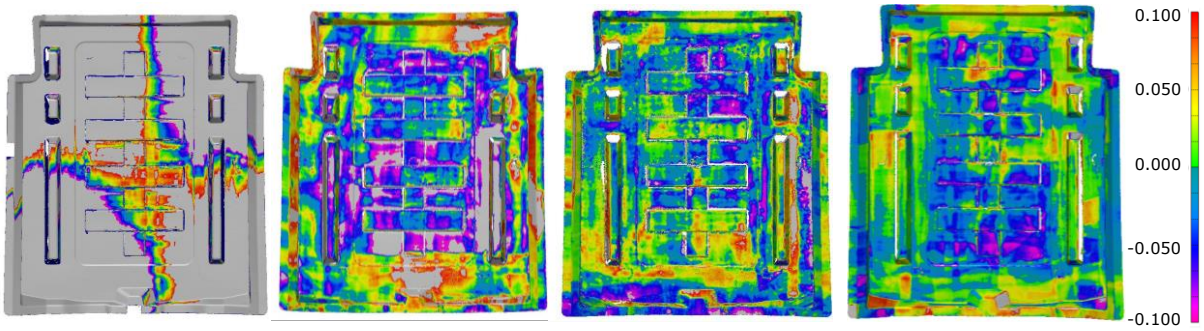

Figure 5: Direct comparison of replicate scans acquired through different scanning techniques (mm): (a) fixtured, (b) free-state on low quality flat table, (c) unclamped on high quality flat table, (d) scenario (c) covered with antireflective coating.

3.2 Accuracy Assessment

Once the repeatability of the process was brought within acceptable limits, the accuracy of the RE process was assessed by means of a reverse engineering validation scheme. The physical part was placed with the larger central flat zone in contact with the high-quality table and the distance between six different flange points (Figure 6a) and the flat surface table were measured by means of a touch trigger height measurement gage (accuracy = ±0.03 mm, repeatability = 0.01 mm). Complementary virtual measurements were determined in a similar manner, but this time by means of the digital model obtained through RE. The location of the inspection points was primarily determined by their accessibility with respect to both physical and virtual measurements. More specifically, the peripheral location of the inspection points was set to enable a facile and consistent placement of the physical measurement gauge, whereas their global distribution was meant to better capture the overall geometry/warpage of the part.

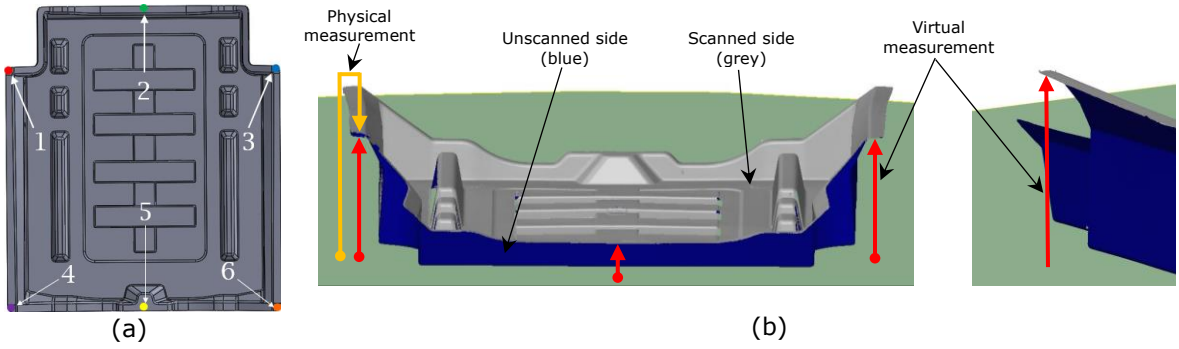

Figure 6: RE validation protocol for SBO: (a) inspection points, (b) validation distance.

3.2.1 Physical measurements

The distance between the upper/scanned surface of the SBO and flat surface of the table was measured by means of the aforementioned height gauge. For this purpose, SBO was laid on the

granite table and the height gauge was moved around the part in order to capture the distances depicted in Figure 6a. Triplicate measurements were taken at each of the six locations (Table 2).

Point Location	Top Left (Point 1)	Top Center (Point 2)	Top Right (Point 3)	Bottom Left (Point 4)	Bottom Center (Point 5)	Bottom Right (Point 6)
Test 1 [mm]	103.39	27.14	103.27	83.25	26.27	83.94
Test 2 [mm]	103.38	27.16	103.33	83.22	26.29	83.89
Test 3 [mm]	103.34	27.17	103.28	83.30	26.28	84.00
Mean [mm]	103.37	27.15	103.29	83.25	26.28	83.94
StDev [mm]	0.026	0.015	0.032	0.040	0.010	0.055

Table 2: Distance to the reference surface in the physical setup.

As the results suggest, data collected was characterized by a high level of consistency.

3.2.2 Virtual measurements

It is important to note here that after extensive efforts were made to determine a flat reference plane exclusively by means of the scanned SBO model, this approach was eventually abandoned. Two factors contributed to this outcome. First, there are numerous RE artifacts in the final SBO mesh that effect the best fitting of the virtual reference plane. Second, the natural position where the part settles is affected by gravity, and not just the local conformation of the surface in contact with the table. When attempting to establish a virtual reference plane it was found that the actual position and orientation was extremely sensitive to the region of the mesh being included in the planar best-fitting. For these reasons, the initial comparisons between virtual and physical measurements were largely discrepant as a consequence of the incorrect positioning of the virtual reference plane. However, the issue of inconsistent virtual reference planes was solved by including a region of the physical table in the original scan of the part and using it to create the virtual reference plane. This enabled consistent and repeatable determinations of the virtual reference plane. More details on this topic will be presented in the upcoming Section 4.3.2.

The second observation to be made with respect to the virtual part model is that only its upper/visible/A side was scanned (Figure 6a). This decision was prompted both by the large number of parts to be reverse engineered (in the hundreds range) as well as the fact that only this side was necessary for the downstream assembly/clamping simulations. While specific registration procedures could have been devised in order to align scans of both sides of the part (both acquired while having the part laying down on the table/flat surface), they were deemed both outside of the scope of the current study and time consuming. Mesh vertices located in the area targeted by the physical measurements were selected for the purpose of distance evaluations. Same as in the physical scenario, triplicate assessments - performed by means of repeated part scans - were used to determine the gaps at the predetermined inspection points. Same as in case of physical measurements a high-level of consistency was observed in the acquired data (Table 3).

Point Location	Top Left (Point 1)	Top Center (Point 2)	Top Right (Point 3)	Bottom Left (Point 4)	Bottom Center (Point 5)	Bottom Right (Point 6)
Scan 1 [mm]	102.975	27.158	103.109	83.315	26.150	83.258
Scan 2 [mm]	103.075	27.183	103.177	83.545	26.202	83.285
Scan 3 [mm]	103.058	27.131	103.263	83.346	26.327	83.320
Mean [mm]	103.036	27.157	103.183	83.402	26.226	83.288
StDev [mm]	0.054	0.026	0.077	0.125	0.091	0.031

Table 3: Distance to the physical reference plane in the virtual setup.

3.2.3 Discussion

Student t-test was used to investigate the level of correlation between physical and virtual inspection metrics. In this context, t-test was used to verify whether the virtual measurements match their physical counterparts. While a larger number of samples (i.e., n = 21) would have strengthen the accuracy findings, it is believed that the size of the set used was sufficient to assess the trends existent in the acquired data. As Table 4 suggests, point 1 (top left) and point 6 (bottom right) seem to exhibit statistically different means between physical and virtual measurements ($p < 0.05$). For the remainder of four points, no statistically significant difference could be identified.

Point Location	Top Left (Point 1)	Top Center (Point 2)	Top Right (Point 3)	Bottom Left (Point 4)	Bottom Center (Point 5)	Bottom Right (Point 6)
Physical Mean [mm]	103.370	27.150	103.290	83.250	26.280	83.940
Virtual Mean [mm]	103.036	27.157	103.183	83.402	26.226	83.288
Difference [mm]	0.334	-0.007	0.107	-0.152	0.054	0.652
p-value	0.003	0.972	0.117	0.173	0.415	0.000

Table 4: Complex geometry: comparison of physical and virtual accuracy.

The largest contributor to this discrepancy is believed to be movement of the part due to the light contact force induced by the tough-trigger jaw of the height gage. This is evidenced by inspecting the points that are located in the vicinity of the physical contact between the composite part and the reference plane (close to the projection of Top Center/Point 2 and Bottom Center/Point 5 onto the reference plane) that seem to yield measurements that are relatively close between physical and virtual measurement scenarios. This observation underscores the challenges associated with obtaining free-state measurements of warped composite components.

Theoretically, the physical contact points between the part and the flat reference plane/surface should be easy to determine. However, part inaccuracies caused by the manufacturing process combined with the artifacts introduced during by the mesh generation process (typically around sharp edges) translate into a difficult task that can only be solved – at least for the time being – through visual and tactile inspection of the physical setup. Nonetheless, the biggest drawback of this approach is that it cannot be automated in the digital environment; whereas, physical observations tend to be confined to the part/surface interface located around the periphery of the part, where a direct line of sight is present. That being said, an overview of all differences that were measured between physical and virtual setup indicates that the largest error found remains under 0.65 mm or 0.8%, assuming the physical measurement as the baseline value.

4 CASE STUDY: SIMPLE GEOMETRY

Since the validation results (Table 4) at points 1 and 6 showed that the differences between physical and virtual measurements were statistically significant ($p < 0.05$) a secondary study was conducted by means of a simple quasi-cuboid geometry. This investigation was meant to eliminate or at least reduce the confounding effects caused by part geometry on scanning accuracy/repeatability. This supplementary evaluation was partly inspired by a study of Campanelli, et al [3]. The same optimized reverse engineering techniques described in Section 3 were used in this case.

4.1 Repeatability Assessment

The results of repeatability evaluation are depicted in Figure 7. According to them, the resulting standard deviation was ±0.041, while deviations ranged from a maximum of +0.154 mm to a minimum of -0.152 mm. These results are quite similar to those achieved in the case of the more complex geometry.

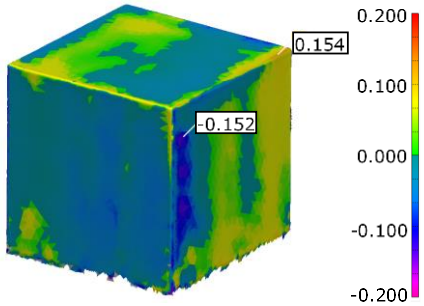

Figure 7: Deviation map between two replicate scans (mm).

4.2 Accuracy Assessment

To validate RE accuracy, triplicate (n = 3) physical caliper-based measurements were conducted for each principal dimension of the cube (Figure 8). Nonetheless, a different measurement strategy had to be employed for the two virtual measurements located in the horizontal plane. In this new approach, the opposite side of the face to be measured was used to generate the virtual reference plane. This plane was then used to calculate the distance between itself and the opposite face of the cube. The plane was generated by best fitting it to scanned data by means of a method similar to the one used to generate the virtual reference plane based on the granite slab (Section 3.1.3). To avoid the errors introduced by the mesh artifacts associated with the edges of the geometry (to be detailed in the upcoming Section 4.3.1), near-edge regions of the faces were excluded from the planar best fitting procedure. In contrast with X and Y dimensions, the vertical Z dimension was measured with respect to the high-quality surface/table in a manner similar to the one described in Section 3.1.3. The results of the virtual measurements are shown in Figure 9 (n = 3).

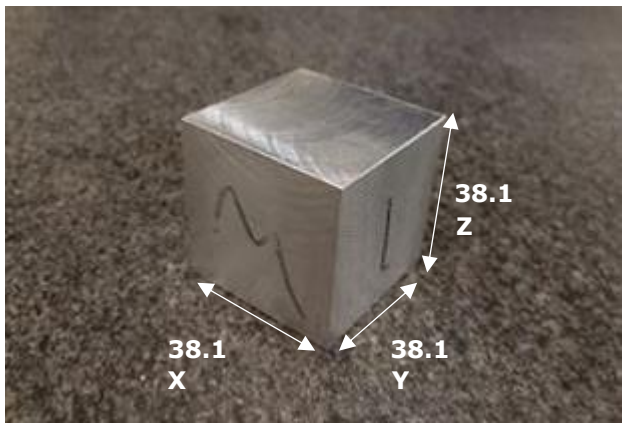

Figure 8: Physical measurements of the cube geometry (mean values in mm).

Same as in Table 4, the results in Table 5 seem to suggest that it is relatively difficult to obtain a match between virtual and physical measurements, essentially implying that the complexity of the geometry is not the only major cause of RE error. By corroborating the data in Tables 4 and 5, it can be speculated that the statistically significant discrepancy obtained at points 1 and 6 (Table 4) could be in fact a consequence of the unintentional movement of the part by the action of the light load exerted by the contact-based measuring device.

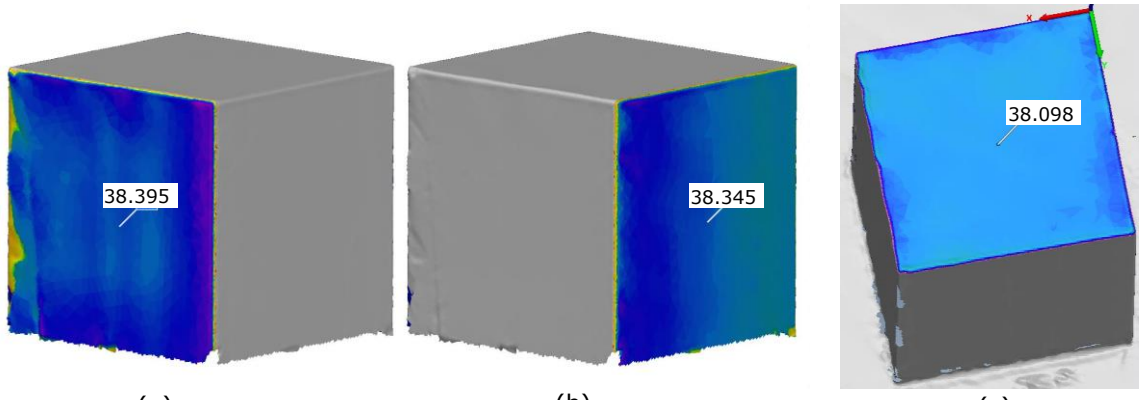

(a) (b) (c)

Figure 9: Virtual measurements of the cube geometry (mean values in mm): (a) X axis, (b) Y axis, and (c) Z axis.

On the other hand, the results in Table 5 imply that the accuracy X and Y axes is lower (lower p values, and higher difference between physical and virtual measurement). This is suspected to be a consequence of the relative angle between the laser beam and the scanned surface [5],[9]. For the scanning of the surfaces used to create the X and Y virtual measurements, the angle of incidence between the laser beam and side surfaces was close to 45°, which was required to avoid hitting the granite surface. As such, with a scanning angle nearer 90°, as in the Z direction, the accuracy is improved (Table 5). Referring to the SBO geometry in Section 3.22, a near 90° scanning angle was also used at points 2 and 5 and resulted in a similar level of accuracy to the Z direction measurement on the block (Table 4).

Measurement	X	Y	Z
Physical Mean [mm]	38.12±0.01	38.14±0.01	38.13±0.00
Virtual Mean [mm]	38.345±0.023	38.395±0.091	38.098±0.020
Difference [mm]	0.225	0.255	0.032
p-value	0.00	0.04	0.11

Table 5: Simple geometry: comparison of physical and virtual accuracy (error bars represent one standard deviation).

4.3 Effect of Mesh Artifacts

In addition to the angle of incidence between the laser beam and the scanned surface, it was suspected that certain mesh artifacts introduced by the tessellation process itself could also introduce errors in the RE process. Unlike some of the previously described error types that affect the quality of the point cloud acquired (part stability/rigidity, surface reflectivity, beam incidence angle), this category of errors tends to be more concealed and thereby overlooked more often, especially since the mesh generation process is usually based on robust and well-tested routines. However – as mentioned at the beginning of Section 3.2.2 – mesh artifacts tend to prevent definition of reliable references that are derived from the scanned geometry.

4.3.1 Edge rounding

Unlike the physical object (Figure 8), its virtual replica was characterized by a relatively visible 'filleting' of its edges (Figure 10). This phenomenon was further aggravated by a certain amount of 'pre-fillet' that seemed to depart significantly from the innate planar nature of the cube faces. Various mesh generation settings were tested in order to further reduce this type of artifact, but they were largely unsuccessful.

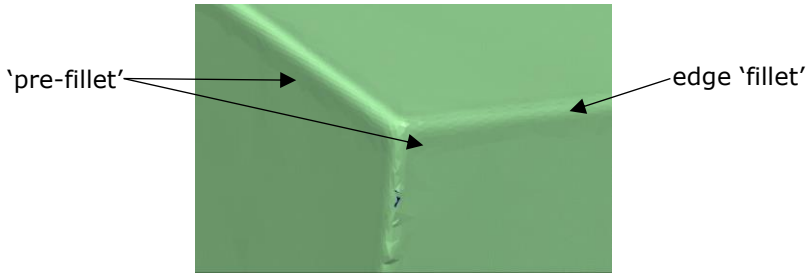

Figure 10: Mesh artifacts present around the edges of the cube geometry.

While it is possible to anticipate that advanced mesh generation algorithms could be developed to mitigate this issue, it is also important to note here that many of the commercial software on the market are unable to do it at this time. Moreover, while alternate solutions could be envisioned for simpler geometries (such as the cube), it is unlikely that robust edge meshing solutions can be developed for complex geometries.

4.3.2 Virtually-generated reference plane

To investigate the effect of mesh artifacts (i.e., 'edge rounding') on the accuracy assessment for a complex part, the B-side of the SBO was scanned (Figure 11). This geometry was required to facilitate the positioning of the virtual reference plane to be derived from it.

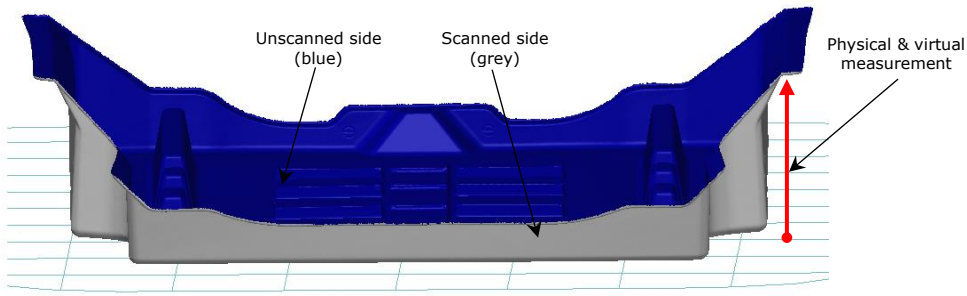

Figure 11: Scan of SBO backside.

The relative position of the plane with respect to the SBO backside is primarily controlled by the percentage of 'outlier points' to be ignored (rejection percentage). More specifically, while a nonzero rejection percentage implies that certain mesh artifacts will be adequately ignored, this also means that the plane will interfere with the reconstructed mesh. Alterations of the rejection percentage will also change the orientation of virtual reference plane, thus changing the virtual measurements. To illustrate this, Figure 12 shows the measurements at the same six measurement points for three distinct outlier rejection percentages. The six analyzed measurement points are the same used in Section 3.2.

Both virtual and physical measurements were performed according to the schematic in Figure 11 and the summary of the results is shown in Table 6. The comparison of these measurements in Table 7 suggests that this method can produce results that are similar to the ones generated by involving a physical reference plane (Table 3). The difference in the absolute values recorded in the two tables is represented by the part thickness that was either excluded (Table 7) or included (Table 3) in the evaluation.

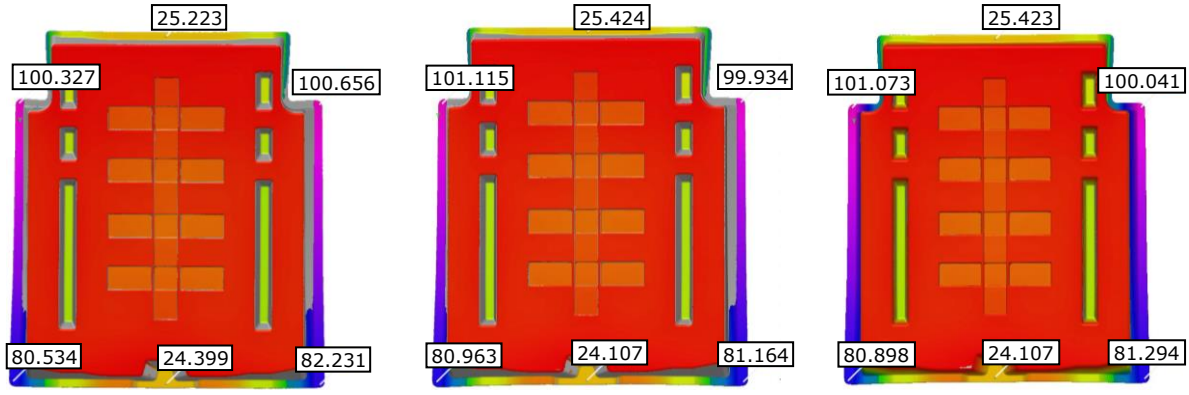

(a) (b) (c)

Figure 12: Virtual measurements involving SBO backside: (a) reject no outliers, (b) reject 0.01% outliers, (c) reject 0.1% outliers.

Point Location	Top Left (Point 1)	Top Center (Point 2)	Top Right (Point 3)	Bottom Left (Point 4)	Bottom Center (Point 5)	Bottom Right (Point 6)
"reject no outliers" [mm]	100.327	25.223	100.656	80.534	24.399	83.231
"reject outliers (0.01% of mesh)" [mm]	101.115	25.424	99.934	80.963	24.107	81.164
"reject outliers (0.1% of mesh)" [mm]	101.073	25.423	100.041	80.898	24.107	81.294

Table 6: Distances to the virtually-generated reference plane.

Nonetheless, the biggest drawback of this approach is that cannot be known *a priori* what is the most appropriate outlier rejection percentage since the 'best' value will largely depends on the (unknown) number of mesh artifacts that were introduced during the RE process.

Point Location	Top Left (Point 1)	Top Center (Point 2)	Top Right (Point 3)	Bottom Left (Point 4)	Bottom Center (Point 5)	Bottom Right (Point 6)
Physical Mean [mm]	100.57	25.24	99.90	80.67	23.98	80.98
Difference "reject no outliers" [mm]	-0.24	-0.01	0.75	-0.14	0.42	1.25
Difference "reject outliers (0.01% of mesh)" [mm]	0.55	0.19	0.03	0.29	0.12	0.19
Difference "reject outliers (0.1% of mesh)" [mm]	0.51	0.19	0.14	0.22	0.12	0.32
Difference [mm]	0.334	-0.007	0.107	-0.152	0.054	0.652

Table 7: Effect of outlier rejection amount on virtual measurements.

Beyond that, variability of the measurements is inherent - caused by the simultaneous modifications of both position and orientation of the virtual reference plane resulting from changing the rejection ratio. Therefore, this approach is less consistent than the approach using the granite table to create the virtual reference plane. Hence, it is inappropriate for accuracy/repeatability evaluation purposes.

5 APPLICATION: WARPAGE ASSESSMENT

The end goal of the previously analyzed RE techniques is the identification of a method capable of producing accurate and repeatable digital replicas of the physical components to be eventually compared with their nominal or CAD counterparts. This type of analysis is required to provide more insight on the stability of the manufacturing process that represents one of the critical components of the quality assurance procedures. Then, as indicated earlier, while CMM-based evaluations remain a *de facto* standard in the industry, there are situations – like the current context – in which their applicability might be regarded as limited.

Since the overall warpage of the composite components represents one of the valuable metrics to be used to assess the consistency of the molding process, a number of measurements were performed in this direction. To ensure the consistency of the reporting, both nominal and warped components were first positioned on a reference plane determined by either the planar back face (CAD part) or the physical high-quality surface used during scanning. The set of points involved in warpage assessment included the six previously analyzed points as well as an additional point in the center (Figure 13). Two series of SBOs (one series per each set of molding conditions) were included in the current warpage assessment summarized in Tables 8 and 9.

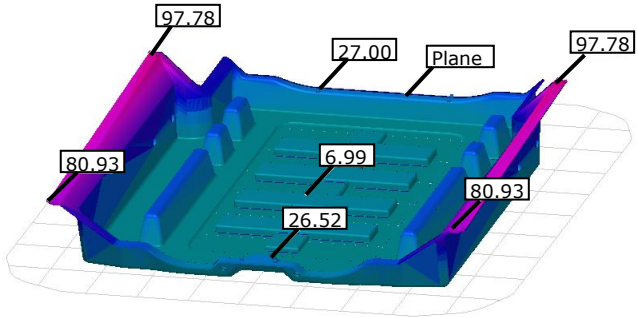

Figure 13: Warpage assessment dataset (seven points).

Part ID	Top Left	Top Center	Top Right	Center	Bottom Left	Bottom Center	Bottom Right
191002-1-1	5.599	-0.045	5.259	5.652	3.421	0.119	1.25
191002-1-2	7.259	0.341	5.473	7.145	9.399	0.946	-0.867
191002-1-3	7.454	0.361	6.328	7.502	6.348	0.543	-0.556
191002-1-4	6.252	0.826	6.371	6.568	4.833	0.634	0.499
191002-1-5	7.267	0.542	6.473	5.719	3.577	-0.083	1.732
191002-1-6	8.673	0.419	6.597	8.811	6.68	-0.633	1.358
191002-1-7	8.022	0.351	7.669	8.082	4.775	-0.256	2.154
191002-1-8	7.503	0.852	6.742	7.565	5.435	0.537	1.931
191002-1-9	5.942	0.984	6.279	7.052	2.858	0.471	5.994
191002-1-10	8.062	0.983	6.659	7.475	1.752	0.321	4.144
191002-1-11	8.055	0.334	7.524	7.731	3.798	-0.427	2.129
191002-1-12	7.482	0.646	6.422	6.299	2.188	0.183	3.445
191002-1-13	6.628	0.376	5.916	6.056	5.298	0.25	1.74
191002-1-14	6.947	0.569	8.044	7.933	1.706	0.372	8.698
Average	7.225	0.539	6.554	7.114	4.433	0.213	1.919
Std Dev	0.877	0.293	0.779	0.941	2.143	0.436	1.842

Table 8: Deviation measurements (mm) for 'Series 1' SBO.

Part ID	Top Left	Top Center	Top Right	Center	Bottom Left	Bottom Center	Bottom Right
191002-2-1	5.472	0.328	4.351	5.196	5.952	0.166	-0.534
191002-2-2	6.77	0.213	5.729	5.956	4.848	0.074	0.913

191002-2-3	7.054	-0.15	6.402	7.721	4.704	-0.699	1.389
191002-2-4	6.601	1.076	7.015	6.275	7.995	0.782	-0.684
191002-2-5	6.497	0.143	6.582	6.42	3.338	-0.36	1.749
191002-2-6	7.466	0.188	5.785	6.479	4.907	-0.665	3.949
191002-2-7	6.776	0.41	5.487	6.736	7.428	0.697	-0.542
191002-2-8	6.337	0.081	5.959	6.359	1.924	0.007	3.826
191002-2-9	6.12	0.631	4.805	5.679	2.844	-0.021	1.707
191002-2-10	6.13	0.578	5.478	6.151	5.235	-0.154	0.334
191002-2-11	6.692	0.171	5.043	5.939	5.796	0.424	-0.398
191002-2-12	6.584	0.273	5.648	6.212	3.345	-0.241	1.528
191002-2-13	5.717	0.31	4.834	5.391	5.452	0.612	-0.065
Average	6.478	0.327	5.624	6.193	4.905	0.048	1.013
Std Dev	0.533	0.303	0.758	0.634	1.739	0.483	1.562

Table 9: Deviation measurements (mm) for 'Series 2' SBO.

Further to that, Student's t-test (95% confidence interval, $p < 0.05$) was used to determine if the populations associated with the two SBO series were statistically different (Table 10). Statistical significance in this context implies that the change in mold temperature from 100°C to 150°C has an important effect on the warpage associated with a particular assessment point, whereas the lack of statistical significance implies that the analyzed molding conditions have a non-discernable effect on the warpage characteristic to those part locations.

Location	Series 1 Mean Measurements (± StDev)	Series 2 Mean Measurements (± StDev)	Difference Between Means	p value
Top Left	7.225 ± 0.877	6.478 ± 0.533	0.746	0.013
Top Center	0.539 ± 0.293	0.327 ± 0.303	0.211	0.078
Top Right	6.554 ± 0.779	5.624 ± 0.758	0.930	0.004
Center	7.114 ± 0.941	6.193 ± 0.634	0.920	0.006
Bottom Left	4.433 ± 02.143	4.905 ± 1.739	0.472	0.534
Bottom Center	0.213 ± 0.436	0.048 ± 0.483	0.165	0.363
Bottom Right	1.919 ± 1.842	1.013 ± 1.562	0.906	0.098

Table 10: Comparison between the warpage patterns associated with the two series (Series 1, n = 14; Series 2, n = 13).

The graphical representation of the data in Table 10 is given in Figure 14 (error bars represent one standard deviation).

According to these results, measurement locations exhibiting statistically significant differences were: Top Left, Top Right, and Center locations ($p < 0.05$). Thus, at these points, the two series of parts can be differentiated, and at the remaining four measurement points the two series of parts cannot be differentiated. It is important to note, even though the error bars are overlapping at the Top Left, Top Right and Center locations, these points can be differentiated using statistics. The range of differences between the means at the three points that show statistical differences is 0.746 mm to 0.930 mm. In the context of ultrasonic welding, this may make a practical difference between what is weldable and what is not, however this is subject to further investigation.

The measurements and error for top and bottom center points indicate that the warpage at these locations is relatively low. Furthermore, at these points the similarity of the two population means demonstrates that even when processing conditions are changed, the resulting warpage does not change significantly. Conversely, the large error bars associated with bottom left and bottom right locations suggests that the variation of warpage for intra-series parts is much larger than at the

other locations. The large range of the measured warpage could be a sign that even the large differences between the means could be in fact attributed to random error. These large distributions of the warpage values hint that even large differences between means at these locations can be attributed to random error.

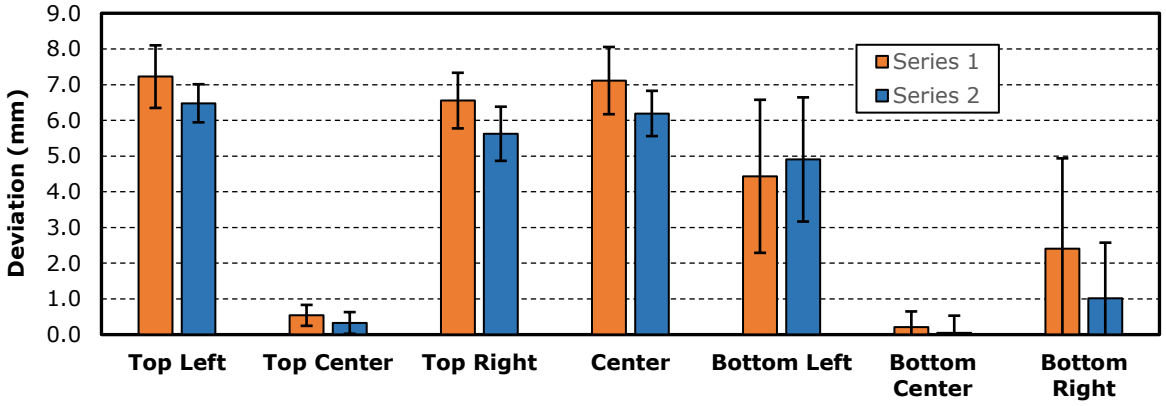

Figure 14: Summary of deviation comparison between series 1 and series 2.

6 CONCLUSIONS

The main objective of this study was to perform an assessment of the repeatability and accuracy associated with the RE process as applied to warped composite parts. Once evaluated, these factors have been used to select a RE technique capable of ensuring precise and consistent comparisons between the molded components and their nominal (CAD) counterpart.

Unlike much of the previously reported work in this area, the particularities of analyzed parts have prompted this study to focus on free-state scanning by demonstrating the possible negative effects of inadequate fixturing. Based on the acquired results, one possible strategy to obtain high quality and consistent digital replicas of the physical warped components involves free-state scanning of the white-powder coated part placed on high quality flat surface. The repeatability and accuracy assessments performed in this setup revealed that: i) paired comparisons of replicate scans place 98.5% of the scanned points (generally in the range of one-two million per part) within a tolerance of 0.141 mm (3σ) from each other, and ii) levels of accuracy within 0.054 mm between physical and virtual measurement are attainable. Additional test scans performed on a simple cube geometry revealed that while part complexity does not play a big role on the accuracy/repeatability of RE, laser beam incidence angle might matter.

The developed RE technique was further used to compare the warpage pattern of two series of molded parts. While some measurement points (top right, top left, and center) showed discernable differences ($p < 0.05$) in warpage, further investigation is required to determine if the differences ($\sim$1 mm) have practical relevance on the downstream assembly process. Deviations at top and bottom center locations had the lowest standard deviation (and therefore lower part-to-part variability) although the warpage at these locations did not show discernable differences ($p > 0.05$) between the two series. Finally, the remaining two measurement locations (bottom right and bottom left) showed high part-to-part variability within a series of part molded with the same conditions (standard deviation as high as 2.143 mm) and thereby therefore no definite conclusion with respect to warpage can be drawn for these two points. While additional studies would be required to narrow down the root causes of these part inconsistencies, it is likely that the observed part variation is determined by process parameters such as: cooling properties of the mold, fiber orientation, and geometry of the part or charge placement. While separate studies would be required to narrow down the root causes of these part inconsistencies, some of the common factors that could be cited in this

context are variability in the following: cooling properties of the mold, fiber orientation, geometry of the part or charge placement.

Future extensions of this work will attempt to use the RE tools developed in this work in order to perform a more in-depth investigation of the factors with a prominent effect on part-to-part variation as well as their possible mitigation measures. Furthermore, additional studies could investigate the effect of scanner performance and part geometry on the accuracy and repeatability of the entire reverse engineering process. Undoubtedly, without being all-inclusive in this regard, the current study could become a valuable baseline for any future studies focused on similar topics.

ACKNOWLEDGEMENTS

The work presented in this study is the result of the collaboration between Western University (London, Ontario, Canada) and General Motors of Canada. Financial support was provided by Ontario Centers of Excellence (OCE), Natural Sciences, Engineering Research Council (NSERC) of Canada, General Motors of Canada, and Western University.

ORCID

Eric J. Martin, https://orcid.org/0000-0002-6513-0055
O. Remus Tutunea-Fatan, https://orcid.org/0000-0002-1016-5103
Ryan Gergely, https://orcid.org/0000-0003-0351-9177
David A. Okonski, https://orcid.org/0000-0003-0485-6749

REFERENCES

[1] Ameen, W.; Al-Ahmari, A.; Hammad Mian, S.: Evaluation of handheld scanners for automotive applications, Applied Sciences, 8(2), 2018, 217. http://dx.doi.org/10.3390/app8020217

[2] Besic, I.; Van Gestel, N.; Kruth, J.-P.; Bleys, P.; HodoliÄ□, J.: Accuracy improvement of laser line scanning for feature measurements on CMM, Optics and Lasers in Engineering, 49(11), 2011, 1274-1280. http://dx.doi.org/10.1016/j.optlaseng.2011.06.009

[3] Campanelli, V.; Howell, S. M.; Hull, M. L.: Accuracy evaluation of a lower-cost and four higher-cost laser scanners, Journal of biomechanics, 49(1), 2016, 127-131. http://dx.doi.org/10.1016/j.jbiomech.2015.11.015

[4] Cuesta, E.; Alvarez, B.; Martinez-Pellitero, S.; Barreiro, J.; Patiño, H.: Metrological evaluation of laser scanner integrated with measuring arm using optical feature-based gauge, Optics and Lasers in Engineering, 121, 2019, 120-132. http://dx.doi.org/10.1016/j.optlaseng.2019.04.007

[5] Gerbino, S.; Del Giudice, D. M.; Staiano, G.; Lanzotti, A.; Martorelli, M.: On the influence of scanning factors on the laser scanner-based 3D inspection process, The International Journal of Advanced Manufacturing Technology, 84(9-12), 2016, 1787-1799. http://dx.doi.org/10.1007/s00170-015-7830-7

[6] Iuliano, L.; Minetola, P.; Salmi, A.: Proposal of an innovative benchmark for comparison of the performance of contactless digitizers, Measurement Science and Technology, 21(10), 2010. http://dx.doi.org/10.1088/0957-0233/21/10/105102

[7] Kovacs, L.; Zimmermann, A.; Brockmann, G.; Gühring, M.; Baurecht, H.; Papadopulos, N.; Schwenzer-Zimmerer, K.; Sader, R.; Biemer, E.; Zeilhofer, H.: Three-dimensional recording of the human face with a 3D laser scanner, Journal of plastic, reconstructive & aesthetic surgery, 59(11), 2006, 1193-1202. http://dx.doi.org/10.1016/j.bjps.2005.10.025

[8] Kuş, A.: Implementation of 3D optical scanning technology for automotive applications, Sensors, 9(3), 2009, 1967-1979. http://dx.doi.org/10.3390/s90301967

[9] Mahmud, M.; Joannic, D.; Roy, M.; Isheil, A.; Fontaine, J.-F.: 3D part inspection path planning of a laser scanner with control on the uncertainty, Computer-Aided Design, 43(4), 2011, 345-355. http://dx.doi.org/10.1016/j.cad.2010.12.014

[10] Martínez, S.; Cuesta, E.; Barreiro, J.; Alvarez, B.: Methodology for comparison of laser digitizing versus contact systems in dimensional control, Optics and Lasers in Engineering, 48(12), 2010, 1238-1246. http://dx.doi.org/10.1016/j.optlaseng.2010.06.007
[11] Martínez, S.; Cuesta, E.; Barreiro, J.; Álvarez, B.: Analysis of laser scanning and strategies for dimensional and geometrical control, The International Journal of Advanced Manufacturing Technology, 46(5-8), 2010, 621-629. http://dx.doi.org/10.1007/s00170-009-2106-8
[12] Michaeli, J. G.; DeGroff, M. C.; Roxas, R. C.: Error aggregation in the reengineering process from 3D scanning to printing, Scanning, 2017, 2017. http://dx.doi.org/10.1155/2017/1218541
[13] Pereira, J. R. M.; de Lima e Silva Penz, I.; da Silva, F. P.: Effects of different coating materials on three-dimensional optical scanning accuracy, Advances in Mechanical Engineering, 11(4), 2019. http://dx.doi.org/10.1177/1687814019842416
[14] Segreto, T.; Bottillo, A.; Teti, R.; Galantucci, L. M.; Lavecchia, F.; Galantucci, M. B.: Non-contact reverse engineering modeling for additive manufacturing of down scaled cultural artefacts, Procedia CIRP, 62(2017), 2017, 481-486. http://dx.doi.org/10.1016/j.procir.2017.03.042
[15] Sherman, L. M.: Portable 3D laser scanner slashes molder's inspection time, Plastics Technology 61(11), 2017, 72. https://search.proquest.com/docview/1966055851?accountid=15115&pq-origsite=summon
[16] Wang, Y.; Feng, H.-Y.: Effects of scanning orientation on outlier formation in 3D laser scanning of reflective surfaces, Optics and Lasers in Engineering, 81(2016), 2016, 35-45. http://dx.doi.org/10.1016/j.optlaseng.2016.01.003